J Mater Sci (2007) 42:2603–2611
DOI 10.1007/s10853-006-1340-9

Characteristics of nanostructure and electrical properties of Ti thin films as a function of substrate temperature and film thickness

H. Savaloni · K. Khojier · M. S. Alaee

Received: 24 December 2005 / Accepted: 6 March 2006 / Published online: 2 January 2007
© Springer Science+Business Media, LLC 2006

Abstract Titanium films of different thickness at different substrate temperatufres are prepared using PVD method. The nanostructure of these films was obtained using X-ray diffraction (XRD) and AFM, while the thicknesses were measured by means of Rutherford back scattering (RBS) technique. Resistivity, Hall coefficient, concentration of carriers and the mobility in these films are obtained. The results show that, the rutile phase of TiO_2 is formed which is initially amorphous and as the film thickness increases it tends to become textured in (020) direction, which is more pronounced at higher temperatures and possibly transforms to anatase TiO_2 with (112) orientation for thickest films of 224 nm. The conductivity and concentration of carriers increase with thickness, while the Hall coefficient and the mobility decrease. The activation energies in these samples were obtained from the Arrhenius plots of σ and R_H. For thinner films ($E_a \approx 0.4 - 0.6$ eV) and for thickest film (224 nm) a break point is observed at about 500 K, which is consistent with the idea of more processes becoming activated at higher temperatures.

H. Savaloni (✉) · M. S. Alaee
Department of Physics, University of Tehran,
North-Kargar St., Tehran, Iran
e-mail: savaloni@khayam.ut.ac.ir

H. Savaloni · K. Khojier
Plasma Physics Research Center, Science and Research
Campus of Islamic Azad. University, P. O. Box 14665-678,
Tehran, Iran

Introduction

Titanium and its nitride coatings are used as protective coatings against wear and corrosion [1–3] as well as optical and decorative coatings [4–6]. Titanium films are also used as a biomaterial or medical devices or dental application due to its superior performance [7].

Organic waste removal from water and air by semiconductor photocatalytic treatment, using systems based on titanium dioxide, TiO_2, in thin films and nanocrystalline form, has been a subject of considerable interest in the last few years as a low-cost material in photocatalysis [8–10], in photovoltaics [11, 12], or as gas sensors [13, 14]. For example, when used for photocatalytic treatment usually reduces toxic organic compounds to non-toxic inorganic compounds, such as carbon dioxide, water, ammonium or nitrides, and chloride ions. The thin film technique is becoming a standard for the preparation of TiO_2-based photocatalysts. One of the advantages of the thin film photocatalysts is that the catalysts layer may be connected to an external power source to reduce the recombination of UV-activated electrons and holes and increase the catalyst efficiency [15]. In most research work in photocatalysis carried out up to now, TiO_2 has been used in the form of powder particles, often dispersed in solution. On the other hand, for many applications a more suitable form of a TiO_2 photocatalyst would be a (thin) film strongly bound to a substrate such as glass or ceramic [16].

For optimal performance of devices, these films should have special properties. Different properties of thin films are strongly influenced by the nano-structure of films such as grain sizes, nano-strain, crystallographic orientation and other features. It is shown that

nano-structure of thin films are strongly affected by film preparation procedures and deposition condition. For example substrate temperature [17–20], angle of incidence [21–23], deposition rate [24–26], and film thickness [26, 27] have important effects on the morphology and nano-structure of thin films.

Among the modern methods of thin solid film preparation, the physical vapor deposition (PVD) is one of the most flexible, applicable to the preparation of doped films or multilayer structures. In this paper we have shown that, how easily one can obtain TiO_2 films with a (020) preferred orientation through deposition of Ti in a vacuum of ~10^{-5} mbar without any need for presence of extra oxygen during deposition or further treatments such as annealing after deposition. For this we are in debt of the gettering property of titanium and decomposition of water in the vacuum chamber at higher temperatures. The structural and electrical properties of TiO_2 films produced are characterized.

Experimental details

Titanium films of 53–224 nm thickness were produced by resistive evaporation from W boats, at substrate temperatures of 380–580 K. The purity of titanium was 99.98%. An Edwards (Edwards 360) coating plant with a base pressure of 5×10^{-5} mbar was used. The pressure during evaporation was typically about 2×10^{-5} mbar, owing to the gettering property of Ti. In order to keep the evaporation condition for all substrates and temperatures constant, a substrate system with a solar system configuration was designed and constructed, in which up to six substrate holders (planets) were able to move on six arms from the center of the system, providing positions for different angles of incidence, and rotate about cylinder axis and the main (solar) system axis, providing uniform deposition. Detailed description of this system is given in our earlier work [22]. On each copper disk substrate holder the substrate (a disk of 25 mm diameter and 1.0 mm thickness glass cut from microscope slides, or $22 \times 22 \times 0.15$ mm thick glass cover slips) can be fixed by a stainless steel mask. The substrate temperatures were controlled by programmed thermostats and thermocouples fixed inside a hole on the surface of copper disk substrate holder.

Just before use all glass substrates were ultrasonically cleaned in heated acetone then ethanol. The surface texture of the substrates was measured by a Talysurf profilometer. The rms substrate roughness R_q for both kinds of glass substrates was 0.3 nm. The substrate positions were chosen, so that their normal to the direction of incidence of the evaporant beam was at 10° and the distance between the center of the evaporation boat and the center of the substrate holder system was 20 cm. In order to provide a point source for geometrical reasons, a plate of W with a 5 mm diameter hole in the middle was used as a mask (cap) on top of the evaporation boat. In this way, six films can be produced at six different substrate temperatures, under the same evaporation condition, in one evaporation run. The deposition process was repeated several times and reproducibility of the results was confirmed. Film thickness was measured using the RBS technique. A typical RBS spectrum of 64 nm Ti film produced at 503 K is given in Fig. 1. The electrical resistivity and the Hall coefficient of Ti films were measured using a 4-point probe and a Hall effect measurement system with a magnetic field strength of 2500 Gauss, respectively. The nanostructure of these films was obtained using a Philips XRD X'pert MPD Diffractometer (Cu K_α radiation) with a step size of 0.03° and count time of 1 s per step, while the surface physical morphology and roughness was obtained by means of AFM (Park Scientific) analysis. The details of samples produced for investigation in this work, surface roughness, electrical parameters, peak position in the XRD pattern and related d-spacings obtained are given in Table 1.

Results

Nanostructure of the films

Polycrystalline films deposited on substrates generally show preferred orientation, with a strength which depends on the deposition method, film material, and deposition conditions. Savaloni et al. [28, 29] found a

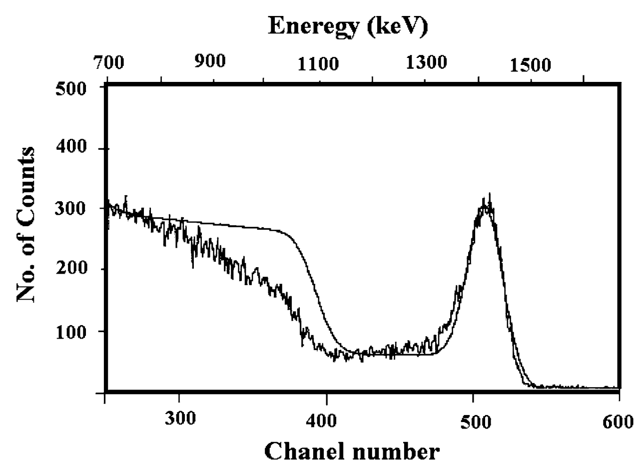

Fig. 1 RBS spectrum of 64 nm Ti film deposited on glass substrate at 503 K substrate temperature

Table 1 Details of samples investigated and the electrical parameters obtained

Sample no.	Group	t (nm)	T_s (K)	$2\theta°$	R_q (Å)	R_{av} ($\mu\Omega$ cm)	R_H (cm^3 A^{-1} s^{-1})	μ (m^2 v^{-1} s^{-1}) × 10^4	n (cm^{-3}) × 10^{18}
Ti1	I	53	387	a	36.7	330	2.37	0.71	2.6
Ti2		64	387	a	27.2	287	1.96	0.68	3.1
Ti3		77	387	38.17	23.4	153	1.02	0.66	6.2
Ti4		224	387	38.80	19.0	132	0.79	0.59	7.9
Ti5	II	53	473	a	29.1	274	1.54	0.61	4.0
Ti6		64	473	38.03	48.1	204	1.21	0.56	5.1
Ti7		77	473	38.31	47.1	116	0.80	0.59	7.8
Ti8		224	473	38.32	53.6	102	0.35	0.35	17.2
Ti9	III	53	503	38.32/64.58	7.1	210	1.35	0.64	4.4
Ti10		64	503	38.19/76.80	9.4	201	0.99	0.49	6.0
Ti11		77	503	38.20/64.62/77.1	12.5	86	0.42	0.49	14.8
Ti12		224	503	38.42	28.1	66	0.11	0.17	53.6
Ti13	IV	53	579	a	5.2	174	0.93	0.53	6.7
Ti14		64	579	38.16	24.6	151	0.52	0.34	12.1
Ti15		77	579	38.20	28.1	76	0.27	0.35	23.1
Ti16		224	579	38.52	32.3	39	0.06	0.14	124.0

t, film thickness; T_s, substrate temperature; R_q, film surface roughness; R_{av}, average resistivity; R_H, Hall coefficient; μ, mobility of carriers; n, number of carriers; a, amorphous

(002) preferred orientation in erbium (hcp, rare earth metal) thin films produced by electron gun evaporation, which reached its maximum at 575–775 K substrate temperature and was stronger for higher deposition rate of 2.5 nm/s compared with 0.55 nm/s. Huang et al. [30] in comparing an evaporated thin Ag (fcc, noble/transition metal) film with Ag film produced using Ar ion bombardment concluded that the latter shows much less (111) preferred orientation. Savaloni and Bagheri Najmi [22] also found a (002) preferred orientation for Zn (hcp, transition metal) films on glass and stainless steel substrates which reached a maximum at about 400 K for Zn/glass and a maximum at about 370 K for Zn/SS, while a (111) preferred orientation for Cu (fcc, noble/transition metal) on glass and SS films reached its maximum at about 590 K for Cu/glass and at about 560 K for Cu/SS. Both Zn and Cu films were produced by resistive evaporation technique and at a pressure of 10^{-5} mbar. They also discussed the effect of residual gas and degassing of substrates (i.e., glass and SS) on the preferred orientation. Savaloni et al. [27] also observed strong (100) preferred orientation for Ti/glass sputtered films.

Titanium dioxide can be formed in three crystalline modifications, anatase, brookite and rutile [31]. It should be noted that other oxides, Ti_2O, TiO, Ti_2O_3, Ti_3O_5 and Ti_nO_{2n-1} (n = 4–10) (Magneli phases) may be formed at low oxygen concentrations. The anatase TiO_2 is more stable than the rutile form for the temperatures lower than 800 °C. The phase transition anatase $\rightarrow$ rutile occurs at 800 °C, when a sample is heated; on cooling, the back transition does not occur because of the high activation energy.

Many authors have tried to characterize the TiO_2 films using X-ray diffraction (XRD) and/or transmission electron microscopy (TEM) [32–36]. TiO_2 films produced by reactive evaporation or PECVD methods are characterized by a lower density and grow in amorphous state below 573 K [37, 38] (our samples (Table 1) are produced at lower or about this temperature). On the other hand, sputtering and ion beam assisted deposition, i.e., methods characterized by higher particle energies, can produce both amorphous, and crystalline TiO_2 films below 473 K. The published results of experimental studies using these deposition methods are, however, different and in some cases show contradictory results. For example, Meng et al. [39] reported only the anatase structure for a wide range of working pressure, while Okimura et al. [40] observed the phase transition with increasing pressure, and Kazunori et al. [41] obtained single crystalline rutile TiO_2 on sapphire (0001) and (11′20) substrates. Tokuda et al. [42], using RF sputtering deposition on glass substrate at 573 K substrate temperature found a structural dependence on film thickness; 56 and 84 nm films were amorphous, 112 and 140 nm thick films were rutile polycrystalline, and 280 nm thick film was a mixture of rutile and anatase polycrystalline structure.

Typical examples of X-ray phase analysis of the titanium films of different thicknesses are given in Fig. 2a, b for films prepared at 387 and 503 K substrate temperatures, respectively, while the peak position ($2\theta°$) in the XRD pattern for each sample is given in Table 1. Our results ($2\theta°$) in general are consistent with TiO_2 rutile phase, including the diffraction lines of (020) (($2\theta°$ = 38.14); JCPDS Card: 48-1278), (310) and (202)

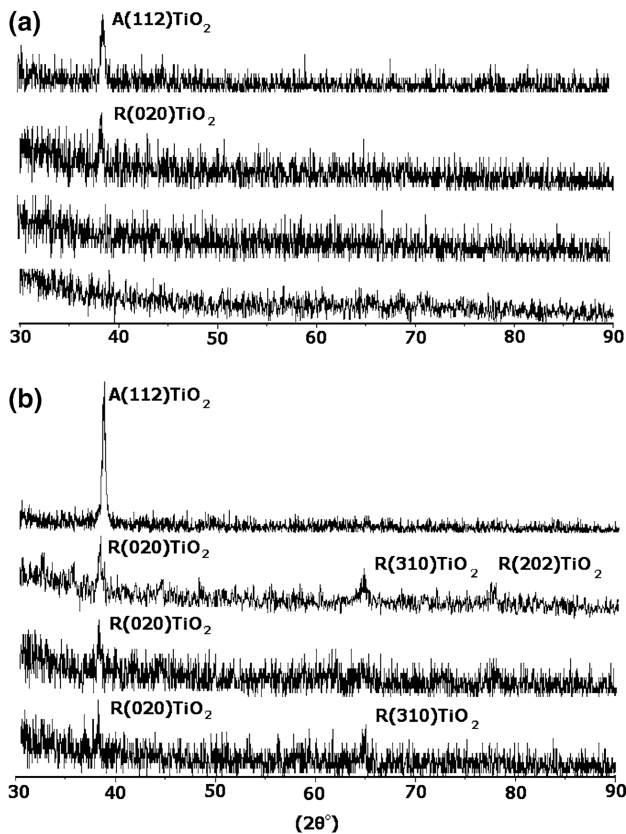

Fig. 2 XRD patterns of TiO_2 films produced at (**a**) 387 K; (**b**) 503 K substrate temperatures for films of different thickness

(($2\theta° = 64.038$) and ($2\theta° = 76.508$), respectively; JCPDS Card: 21-1276), considering the shift of peak position due to stress developed in the film structure and the uncertainty in determining the peak position due to poor intensity. However, there exists an exception for thickest films of groups I, II and III which can possibly be assigned to (112) lattice plane of the anatase phase of TiO_2 with reference to JCPDS Cards: 02-0406 ($2\theta° = 38.969$) and 21-1272 ($2\theta° = 38.575$). One should also point out that the diffraction line of (110) β-Ti with ($2\theta° = 38.482$) though is close to the latter cases but with respect to the rutile phase obtained for thinner films in all groups, there should be high doubt in transformation of oxide film to metallic by increasing film thickness. The structure in lower thicknesses is so weak that can also be considered as amorphous structure, similar to Tokuda et al. [42] results, who used RF sputtering from TiO_2 target. It can be seen that, both the film thickness and the substrate temperature have direct influence on the phase formation and the preferred orientation of titanium oxide films. This shows that, despite the discussion of the preceding paragraph, in fact it is possible to produce rutile TiO_2 films with (020) preferred orientation, by simple resistive evaporation of Ti at a pressure of ~10^{-5} mbar, without any need for using more complicated techniques, such as dc magnetron sputtering with reactive oxygen gas [43], deposition from solution using microwave heating [44] or CVD [45]. This should be as a result of decomposition of water in the vacuum chamber (particularly around the heated substrate holder) and the gettering property of titanium. Savaloni et al. [28], used a quadrupole mass spectrometer and analyzed the partial pressure of the residual gas inside their UHV chamber (base pressure of 10^{-10} mbar; evaporation pressure of 10^{-8} to 10^{-7} mbar) before and after deposition of erbium as a function of substrate temperature. They reported that the substrate holder assembly is an important site for out gassing and for reactions, including those between deposited erbium and residual gases. In particular they found that water decomposes at about 600 K (see Fig. 4 in Ref. [26]). They suggested that the water and its products arise from out gassing and reactions at the substrate and substrate holder. They also related the low partial pressure of oxygen to its rapid reaction with deposited erbium (erbium is also like titanium a powerful getter, but with less gettering effect for oxygen and much higher gettering effect for hydrogen [46]).

With regard to the formation of TiO_2 films in this study, one should consider the following points:

a) the pressure in our chamber (i.e., ~10^{-5} mbar) is much higher than Savaloni et al.'s work [28]. Therefore, there should be much higher partial pressure for residual gases, in particular for water. Hence at high temperatures (e.g., >500 K) there should be a large amount of oxygen and hydrogen as a result of decomposition of water and out gassing from substrate holder assembly in the vacuum chamber,
b) titanium is a very powerful getter and reacts readily with oxygen [46],
c) at high temperature the oxide is more thermodynamically stable [47, 48]. Therefore, it is possible that by increasing the substrate temperature, the available oxygen around the substrate holder reacts and become gettered by titanium atoms to form various forms of titanium oxide. Increasing the substrate temperature, in addition to the above processes, will increase the diffusion process on the substrate surface, by providing sufficient energy and mobility for titanium dioxide particles to crystallize in higher energy phases of rutile or anatase, so producing domains of TiO_2, as observed in the results (e.g., Figs. 2b, 3, 4).

In Fig. 2a and b, it can be seen that the width of TiO_2 diffraction peak decreases with increasing the film

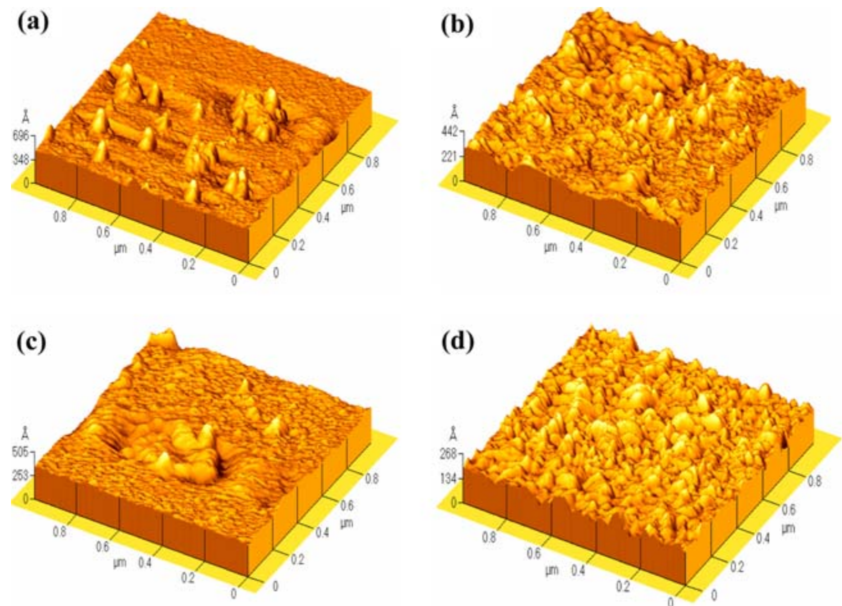

Fig. 3 3D AFM images of TiO_2 films produced at 387 K substrate temperature for different film thicknesses. (**a**) 53 nm, (**b**) 64 nm, (**c**) 77 nm, (**d**) 224 nm

thickness, indicating that the grain size (coherently diffracting domains) increases with film thickness. This in fact may be confirmed by correlating the grain sizes with the conductivity of the film through Arrhenius plots of grain size $\mathrm{GS} \propto \exp(-E_a/KT)$ and conductivity ($\sigma \propto \exp(-(E_a/2KT))$. Figure 6 shows that conductivity or grain size increases with film thickness. This result is also reported by savaloni et al. for erbium [28, 29], and copper and titanium [27] films. Typical 3D AFM images of Ti films of different thickness produced at two different temperatures of 387 and 503 K are shown in Figs. 3a–d and 4a–d. The increase of physical grain size with both film thickness and temperature is also obvious in Figs. 3a–d and 4a–d, and are consistent with the structure zone model predictions [49, 50] and the above discussion. The rms roughness obtained from the AFM analysis for all samples are also given in Table 1. It can be seen that the roughness increases with film thickness for three groups of samples produced at 473, 503 and 579 K substrate temperatures (i.e., groups II, III and IV in Table 1), while samples produced at the lowest substrate temperature of 387 K (group I in Table 1), behave differently (i.e., roughness decreases with

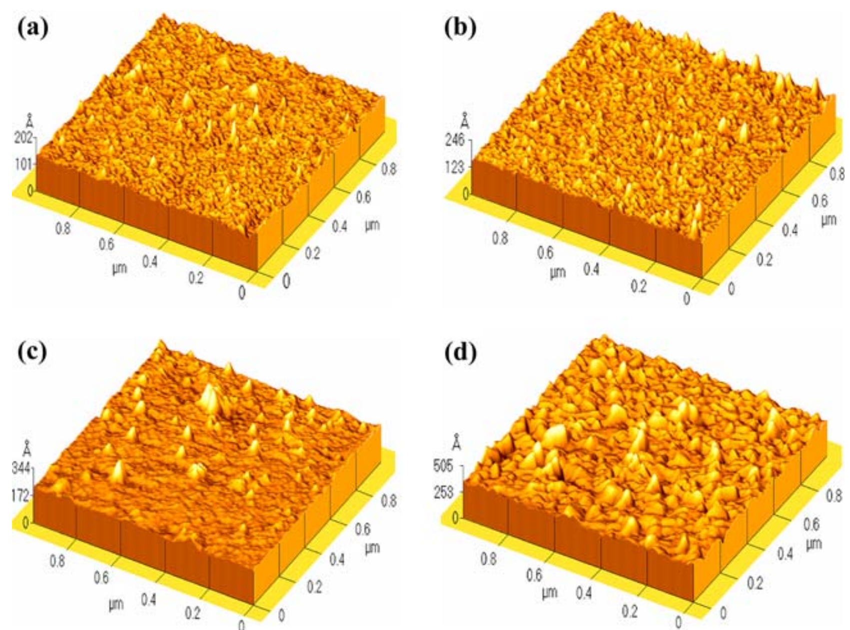

Fig. 4 3D AFM images of TiO_2 films produced at 503 K substrate temperature for different film thicknesses. (**a**) 53 nm, (**b**) 64 nm, (**c**) 77 nm, (**d**) 224 nm

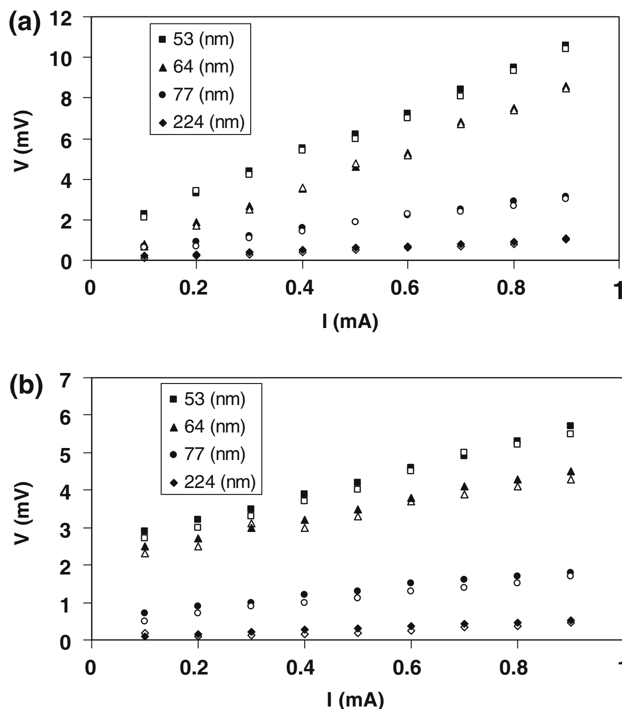

Fig. 5 Variation of voltage as a function of current for TiO_2 films produced at (**a**) 387 K, (**b**) 503 K substrate temperatures for different film thicknesses

increasing thickness). The behavior of the lowest temperature films may be concluded from observation of both XRD patterns (Fig. 2a) and AFM images (Fig. 3a–d), in which amorphous structure is dominant and by increasing thickness, as it is well known [51] the voids/valleys in the film structure fills up and smoother surfaces are produced. On the other hand, as it can be seen in AFM images (Fig. 3a–d) at this temperature the film surface is inhomogeneous, the degree of which decreases with increasing film thickness. This behavior can also be the cause of decreasing roughness in group I of the samples. The reason for the manner in which higher temperature films behave can be explained as follows: for thinner films (XRD results (Fig. 2b), shows an almost amorphous structure), the developed grains are smaller and AFM images (Fig. 4a–d) show an almost a uniform surface, while by increasing the thickness larger grains tend to form (XRD results (Fig. 2b), show the development of TiO_2 (020) rutile crystallographic structure), and in some regions, larger grains stand at higher heights than the rest of the film surface. This can be due to the formation of TiO_2 grains with (020) orientation having a higher rate of growth than the rest of the film [52], owing to the increased diffusion process in higher temperature films.

Electrical properties

In this section, we discuss the results obtained from the measurements of the dc resistivity and the Hall effect. In order to investigate the influence of possible (low frequency) charging effects at the electrical contacts and leads, current–voltage (*I-V*) curves were recorded, scanning the voltage both in increasing and decreasing increments. Figure 5a and b show the results of films of different thicknesses for two different substrate temperatures of 387 and 503 K. However, it should be noted that the current was kept low enough, in order not to heat up the samples. A linear *I-V* curve was obtained, independent of the scan direction, and there was no indication of hystersis effect. In order to investigate the anisotropy effect in our samples, the *I-V* curves measurements were also carried out in four different directions on the samples, namely, two vertical (along the sample length and normal to the length) and two diagonal directions. The values of resistivity for all samples are given in Table 1. The results of resistivity measurements carried out on the thin film samples produced with different film thickness, as expected showed that the resistivity decreases with increasing film thickness at all substrate temperatures examined, and for films of same thickness, the resistivity also decreases with increasing the substrate temperature. The latter behavior is due to the increasing diffusion processes in film and the former is due to the reduction of voids and valleys as the film becomes thicker. Figure 6 presents the variation of electrical conductivity in the form of Arrhenius plot. Linear fits were performed in order to determine the activation energy E_a. Using the mass action law, one can find that the conductivity σ is related to E_a by the expression:

$$\sigma \propto \exp\left(-\frac{E_a}{2K_B T}\right) \quad (1)$$

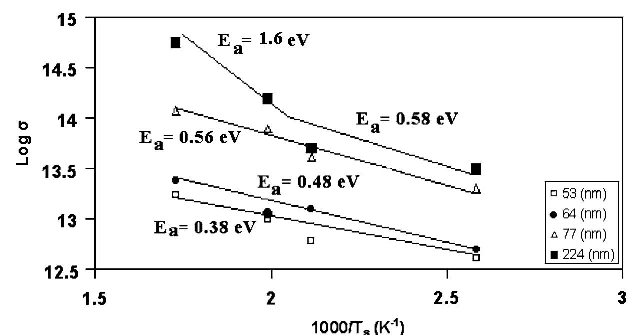

Fig. 6 Arrhenius plot of conductivity

as is indicated on Fig. 6, values of E_a = 0.4–0.6 eV are determined for thinner films of 53, 64, and 77 nm, while there exists a break point for 224 nm thick films at ($T_s \approx 500\,K$; $T_s/T_m = 0.26$). In this case the value of $E_a \approx 0.6\,\text{eV}$ at lower temperatures corresponds to the manner in which thinner films behave (with a gradual increase depending on film thickness), while at higher temperatures the activation energy is increased considerably. This behavior is consistent with our previous results obtained for erbium [28] and copper and zinc [22] films and with the model of Grovenor et al. [52] and with the idea of more processes becoming activated at higher temperatures. In Fig. 6 the influence of thickness at higher temperatures can also be observed.

The Hall's effect is important because it enables us to make measures of mobility and concentration, and gives insight into the mechanism of conductivity in semiconductors. Figure 7a and b and Table 1, show the variation of Hall coefficient, R_H, with film thickness and substrate temperature, respectively. R_H decreases sharply with increasing the film thickness to ~70 nm (Fig. 7a) then this decrease becomes graduated up to the highest thickness of ~224 nm. Figure 7b shows a gradual decrease of Hall coefficient with substrate temperature, which has lowest values for thickest film. In fact the Hall coefficient's behavior is the same as the film resistivity. We can also calculate activation energies from the Hall data, using the formulae $R_H \propto \exp(E_a/K_B T)$. These are given on Fig. 7b. Comparison of the activation energies obtained from the Hall coefficient with those obtained from electrical conductivity in Fig. 6, shows a very close agreement, particularly for thickest films (i.e., 224 nm), with a break point at the same temperature observed in Fig. 6.

The variation of Hall mobility $\mu = \sigma R_H$, with film thickness and substrate temperature is given in Table 1 and shown in Fig. 8a and b. Again the mobility, μ, also decreases with film thickness, while its change with substrate temperature is gradual and shows lowest value for thickest film. The behavior of Hall mobility with temperature suggests that scattering by ionized impurities is the dominant mechanism.

Carrier concentration, n, increases with film thickness, shows a little increase with substrate temperature for films of less than 77 nm thickness (Fig. 9a, b). This change is very pronounced for the thickest film from about 500 K substrate temperature up wards, and in fact shows a break point at a reduced temperature of $T_s/T_m \approx 0.26$; near the zone I to zone II boundary in thin film structure zone model [49, 50]. This break point occurs at the same temperature as it was

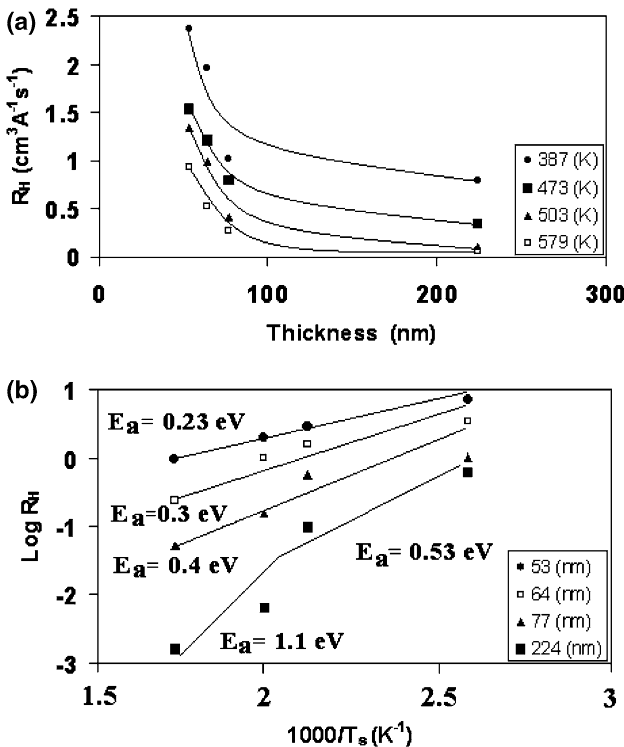

Fig. 7 (a) Variation of Hall coefficient, R_H, with film thickness for TiO_2 films produced at different substrate temperatures. (b) Arrhenius plot of R_H

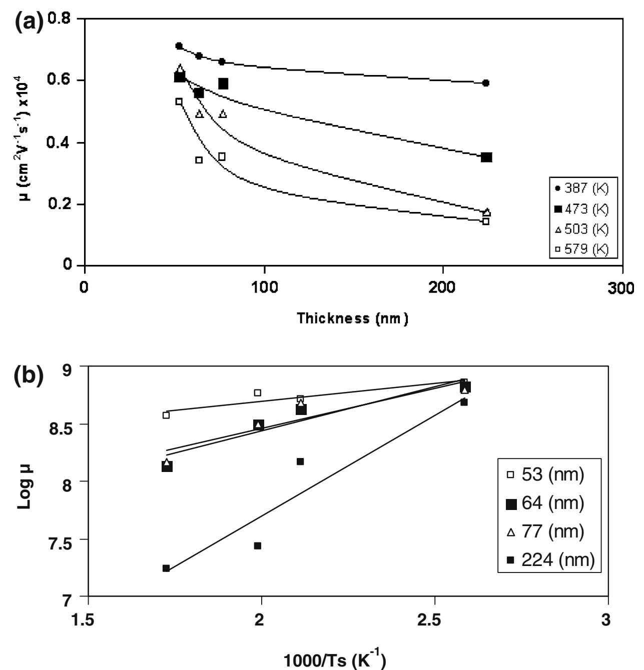

Fig. 8 (a) Variation of mobility, μ , with film thickness for TiO_2 films produced at different substrate temperatures. (b) Arrhenius plot of μ

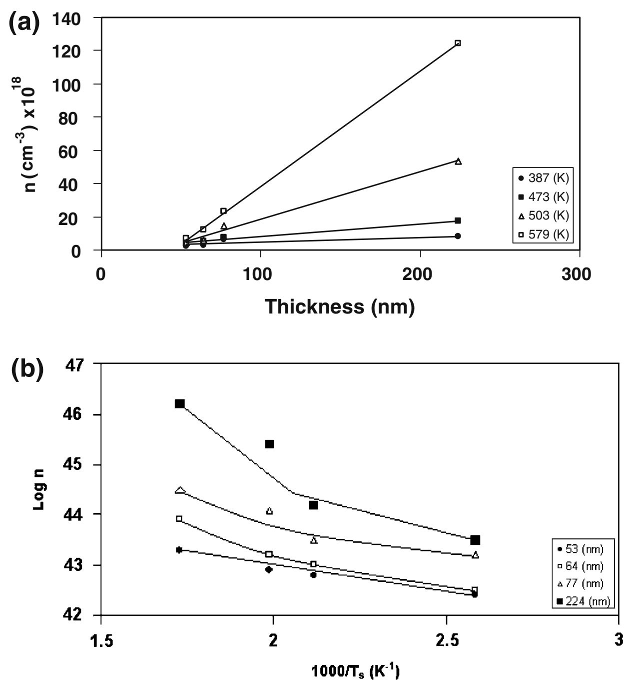

Fig. 9 (**a**) Variation of carrier concentration, n with film thickness for TiO_2 films produced at different substrate temperatures. (**b**) Arrhenius plot of n

observed in Fig. 6 for conductivity (increasing activation energy) and Fig. 7b for Hall coefficient.

Conclusions

TiO_2 rutile and anastase thin films were produced by deposition of Ti (99.98% purity) at 10^{-5} mbar onto glass substrates by resistive technique. It is shown that there is no need for the use of more complicated techniques to produce TiO_2 rutile or anatase phases. The electrical properties of these films (53–224 nm) produced at four different substrate temperatures, are studied. The microstructure of these films, obtained by means of XRD and AFM, showed an increase of grain size, surface roughness and development of (020) orientation by increasing the film thickness. The results of resistivity, Hall coefficient, concentration of carriers and the mobility in these films showed that, conductivity and concentration of carriers increase with thickness, while the Hall coefficient and the mobility decrease. From the exponential dependences of σ on T^{-1} and R_H on T^{-1}, values of the activation energies (0.4–0.6 eV) were derived for thinner films, while a break point for thicker film of 224 nm at ($T_s/T_m \approx 0.26$; the zone I to zone II boundary in structure zone model) is observed, which is consistent with the idea of more processes becoming activated at higher temperatures. This break point is also observed in Arrhenius plot of carrier concentration, n.

Acknowledgements This work was carried out with the support of the University of Tehran and the Plasma Physics Research Centre, Science and Research Campus of I. A. University. We would like to thank the staff at the Nuclear Physics Research Centre of the Atomic Energy Authority of Iran, for their help with the RBS measurements. We are grateful to Ms. M. Shariati of Plasma Physics Research Centre, for AFM measurements.

References

1. Holleck H (1986) J Vac Sci Technol A 4:2661
2. Sundgren J-E, Hentzell HTG (1986) J Vac Sci Technol A 4:2259
3. Milosev I, Navinsek B, Strehblow H-H (1995) In: Corrosion properties of hard PVD nitride coatings (with emphasis on TiN), Scientific Series of the International Bureau, vol 37. GmbH, Forschungszentrum Julich
4. Sikkens M, Heereveld AAMTV, Vogelzang E, Boose CA (1983) Thin Solid Films 108:229
5. Kopacz U, Ried R (1992) Z Metallkd 83:492
6. Claesson Y, Georgson M, Roos A, Ribbing C-G (1990) Solar Energy Mater 20:55
7. Long M, Rack HJ (1998) Biomaterials 19:1621–1639
8. Fox MA, Dulay MT (1993) Chem Rev 93:341
9. Linsebigler AL, Lu G, Yates JT Jr. (1995) Chem Rev 95:735
10. Anpo M, Takeuchi M (2003) J Catal. 216:503
11. Hagfeldt A, Gratzel M (1995) Chem Rev 95:49
12. Gratzel M (2001) Nature 414:338
13. Gopel W, Reinhardt G (1996) In: Baltes H, Gopel W, Hesse J (eds) Sensors update. Wiley, New York, p. 47
14. Skubal LR, Meshkov NK, Vogt MC (2002) J Photochem Photobiol A: Chem 148:103
15. Chang HT, Wu N-M, Zhu F (2000) Water Res 34:407
16. Mills A, Hill G, Bhopal S, Parkin IP, O'Neill SA (2003) J Photochem Photobiol A: Chem. 160:185
17. Savaloni H, Moradi GR, Player MA (2005) Vacuum 77:245
18. Sathyamoorthy R, Narayandass SK, Mangalaraj D (2003) Solar Energy Mater Solar Cells 76:339
19. Toney MF, Lee W-Y, Hedstrom JA, Kellock A (2003) J Appl Phys 93:9902
20. Arranz A, Palacio C (2005) Surf Sci 588(1–3):92
21. Moon K-S, Shin S-C (1996) J Appl Phys 79(8):4991
22. Savaloni H, Bagheri Najmi S (2002) Vacuum 66(1):49
23. Cartier M, Auffret S, Bayle-Guillemaud P, Ernult F, Fettar F, Dienya B (2002) J Appl Phys 91(3):1436
24. Savaloni H, Shahrestani SA, Player MA (1997) Nanotechnology 8(4):172
25. Qiu H, Wang F, Wu P, Pan L, Li L, Xiong L, Tian Y (2002) Thin Solid Films 414:150
26. Cai K, Muller M, Bossert J, Rechtenbach A, Jandt KD (2005) Appl Surf Sci 250(1–4):252
27. Savaloni H, Taherizadeh A, Zendehnam A (2004) Physica B 349:44
28. Savaloni H, Player MA, Marr GV (1992) Vacuum 43:965
29. Savaloni H, Player MA (1995) Vacuum 46:167
30. Huang TC, Lim G, Parmigiani F, Kay E (1985) J Vac Sci Technol A3:2161
31. Clark RJL (1973) In: Bailar SC, Emelens HJ, Trofman-Dickenson AF (eds) Comprehensive inorganic chemistry, vol 3. Pergamon Press, Oxford, pp 375

32. Reece M, Morrell R (1991) J Mater Sci 26: 5566
33. Rickerby DG (1997) Philos Mag B76:573
34. Barbe CJ, Arendse F, Comte P, Jirousek M, Lenzmann F, Shklover V, Gratzel M (1997) J Am Ceram Soc 80:3157
35. Negishi N, Takeuchi K, Ibusuki T, Datye AK (1999) J Mater Sci Lett 18: 515
36. Zeman P, Takabayashi S (2002) Surf Coat Technol 153:93
37. Lobl P, Huppertz M, Mergel D (1994) Thin Solid Films 251:72
38. Frenck HJ, Kulisch W, Kuhr M, Kassing R (1991) Thin Solid Films 201:327
39. Meng LJ, Santos MP (1993) Thin Solid Films 226:22
40. Okimura K, Shibata A, Maeda N, Tachibana K, Noguchi Y, Tsuchida K (1995) Jpn J Appl Phys 34:4950
41. Kazunori F, Gikan T, Iso Y (1993) Jpn J of Appl Phys 1:3561
42. Tokuda K, Miyashita K, Ubukata T, 7th international symposium on sputtering and plasma process (ISSP 2003), pp 96–99
43. Stamate MD (2000) Thin Solid Films 372:246
44. Vigil E, Saadoun L, Ayllon JA, Domenech X, Zumeta I, Rodriguez-Clemente R (2000) Thin Solid Films 365:12
45. Bessergenev VG, Khmelinskii IV, Pereira RJF, Krisuk VV, Turgambaeva AE, Igumenov IK (2002) Vacuum 64:275
46. Muller J, Singh B, Surpplice NA (1972) J Phys D Appl Phys 5:1177
47. Curzon AE (1984) J Less Common Metals 98:149
48. Holloway DM, Swartz WE Jr (1977) Appl Spectrosc 31:167
49. Movchan BA, Demchishin AV (1963) Phys Met Metall 28:83
50. Thornton JA (1975) J Vac Sci Technol 12:830
51. Messier R (1986) J Vac Sci Technol A 4:490
52. Grovenor CRM, Hentzell HTG, Smith DA (1984) Acta Metall 32:773